Realization of a subwavelength focused spot without a longitudinal field component in a solid immersion lens-based system

Kun Huang[1,2] and Yongping Li[1,*]

[1]*Department of Optics and Optical Engineering, University of Science and Technology of China, Hefei, Anhui 230026, China*

[2]*e-mail: huang918@mail.ustc.edu.cn*

**Corresponding author: liyp@ustc.edu.cn*

Received June 14, 2011; revised August 2, 2011; accepted August 11, 2011; posted August 15, 2011 (Doc. ID 149273); published September 6, 2011

In a solid immersion lens (SIL)-based system, we predict theoretically that, by using the illumination of an azimuthally polarized beam with helical phase (APH), the subwavelength focusing can be simultaneously realized both in SIL and the third medium in spite of the presence of an air gap between the SIL and the third medium, which is not easily achieved in the case of the illumination of linearly, circularly, and radially polarized beams. For the APH illumination, the field in the focal region of the multilayered medium has no longitudinal component, and the on-axis intensity of the focused spot is nonzero. The APH illumination extends the capacity of SIL in realizing a supersmall focused spot, which is useful in microscopy, near-field optics, recording optics, and lithographic optics. © 2011 Optical Society of America

OCIS codes: 180.4243, 210.4245, 260.1960, 260.5430.

In a tightly focusing system, the polarization and phase of an incident beam play an important role in reducing the size of the focused spot. Recently, much attention has been given to polarization of the incident beam because cylindrical vector beams [1], especially the radially polarized (RP) beam, have the advantage of obtaining a small focused spot. When focused by a high-NA lens, the RP beam has a strong longitudinal field component with a superresolution size in the focal plane [2]. However, the longitudinal field exhibits its advantage only when the medium in the focal region is homogeneous. In some applications, i.e., optical data storage and optical trapping, the medium is inhomogeneous in the focal region. Taking the solid immersion lens (SIL) system in optical data storage for example, there exist at least three stratified media (immersion lens, air gap, and measured sample) in the focal region. Because the longitudinal field is discontinuous at the interface of adjacent media, its transmission is poor at the interface of low–high (e.g., from air to glass) refractive index media. In addition, the transverse field has higher transmission: as a result, the size of focused spot is enlarged in the measured sample. Therefore, the RP illumination in SIL-based near-field optics is considered to be unsuitable for a near-field information recording or detection system with extremely high imaging resolution [3]. Despite that a complex filter with amplitude and phase modulation is introduced to reduce the transverse field [4], the longitudinal fields' discontinuity at the interface is inevitable. It seems likely that the only method to solve this problem is to find a vector beam that has no longitudinal field component in the focal region when focused by a high-NA lens. To our knowledge, in all the known vector beams, the azimuthally polarized (AP) beam is the only one that meets this requirement. Unfortunately, when focused by a high-NA lens, the AP beam has a ring-shaped intensity profile (with null on-axis intensity) in the focal plane [5]. Therefore, in SIL-based near-field optics, the AP beam is hardly mentioned for realizing a subwavelength focused spot.

Here we introduce azimuthally polarized beam with helical phase (APH) illumination in SIL-based near-field optics to realize a subwavelength focused spot without a longitudinal field component in the focal region. For a focused AP beam, the destructive interference of electric field at the geometric focus leads to null on-axis intensity in the focal region; while for an APH (topological charge $m = 1$), the constructive interference occurs at the geometric focus. The electric field of APH beam can be expressed as $\vec{\mathbf{E}} = A(r)e^{i\varphi}\vec{\mathbf{e}}_{\varphi}$, where $A(r)$ is the angle-independent amplitude, r and φ are the polar coordinates, and $\vec{\mathbf{e}}_{\varphi}$ is the unit vector of angular component. In free space, the APH beam has displayed its potential in decreasing the focal spot size [6].

For simplicity, we investigate a SIL-based system composed of a SIL, air gap and measured sample (Fig. 1) in this Letter. To calculate the vectorial field distribution

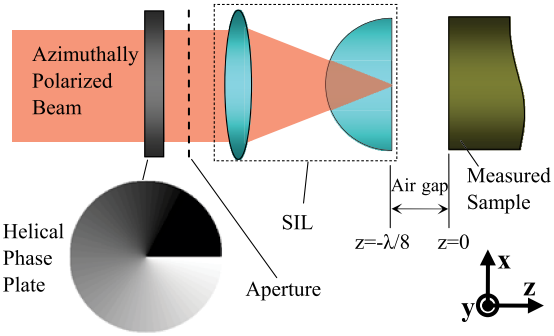

Fig. 1. (Color online) Schematic of the SIL-based system in our analysis. The efficient NA is 1.7 with the 2.0 refractive index (n_{SIL}) of the SIL at a wavelength of 405 nm. The air gap has the thickness of $\lambda/8$. The front interface of the measured sample is at $z = 0$, where the geometric focus of the prefocusing lens locates, which follows the configuration in [4]. For the convenience of drawing, we put the focus at $z = -\lambda/8$ in the sketch. The helical phase plate has the phase distribution with $e^{i\varphi}$.

 © 2011 Optical Society of America

within stratified media in the focal region, we use the efficient algorithm described by van de Nes *et al.* [7] and based on the Richards and Wolf theory [8]. In polar coordinates of (ρ, ϕ, z), the field $(E_{\rho j}, E_{\phi j}, E_{zj})$ in the jth medium is

$$\vec{\mathbf{E}}_j = \frac{-if}{\lambda}\int_0^{\alpha} A(\theta)\sqrt{\cos\theta}(\vec{\mathbf{M}}_j^{+} e_j^{ik_j\cos\theta}\boldsymbol{z} + \vec{\mathbf{M}}_j^{-} e_j^{-ik_j\cos\theta}\boldsymbol{z})\sin\theta \mathrm{d}\theta, \quad (1)$$

where $\alpha = \arcsin(\mathrm{NA}/n_{\mathrm{SIL}}), f$ is the focus of the focusing lens in SIL, θ is the convergent angle in the SIL, and θ_j is the convergent angle in the jth medium that obeys $n_j \sin\theta_j = n_{\mathrm{SIL}}\sin\theta$. $A(\theta)$ is the pupil function of the AP beam that obeys the Bessel–Gauss distribution [5]. $\vec{\mathbf{M}}_j^{\pm}$ are the propagation matrices. For the illumination of the APH beam in this Letter, the propagation matrices in polar coordinates

$$\vec{\mathbf{M}}_j^{\pm} = \pi e^{i\phi}\begin{bmatrix} -i(g_j^{0\pm} + g_j^{2\pm})(J_0 + J_2) \\ (g_j^{0\pm} + g_j^{2\pm})(J_0 - J_2) \\ 0 \end{bmatrix}, \quad (2)$$

where $J_n = J_n(k_{\mathrm{SIL}}\rho\sin\theta)$ and $J_n()$ is the nth Bessel function of the first kind, $g_j^{n\pm}$ are the efficient transmission and reflection coefficients in the jth medium, respectively and are given in [7]. Through the vectorial analysis, the result shows the longitudinal field component E_{zj} is zero in the focal region. However, the integrands of the transverse field components contain the zero-order Bessel function, which means the intensity of the transverse field is nonzero when $\rho = 0$. Therefore, the APH beam has nonzero on-axis intensity in the focal region.

In a computer experiment, we implement the integrals in Eq. (1) using the recursive adaptive Simpson quadrature. When the measured sample has the refraction index $n_{\mathrm{sample}} = 1.5$, the numerical results of fields within the SIL, air gap, and measured sample in the focal region are displayed in Fig. 2. As a comparison, we give the numerical solutions using the RP beam illumination in Fig. 2(a). Because of the discontinuity of the longitudinal field component from the SIL to the air gap, the longitudinal field is largely enhanced in the air gap: as a result, that the peak intensity in the air gap is much larger than those in the SIL ($z < -\lambda/8$) and sample ($z > 0$). When displayed in one figure with the same color scale, the intensity profiles in the SIL and sample are weakened in contrast to that in the air gap. Therefore, in order to clearly show the field in the measured sample, we multiply the real field in air gap by 30% in Fig. 2(a) [3]. However, the field (RP) along the optical axis is real without multiplying the factor of 30% in Fig. 2(c). In the case of APH illumination, the field contains only the transverse component (the radial and azimuthal components in the polar coordinate) in the focal region. Shown in Fig. 2(b), the field is continuous at the interface. As expected, the on-axis intensity in the sample has the maximum in the transverse plane, which is different from the null on-axis intensity in the case of AP illumination.

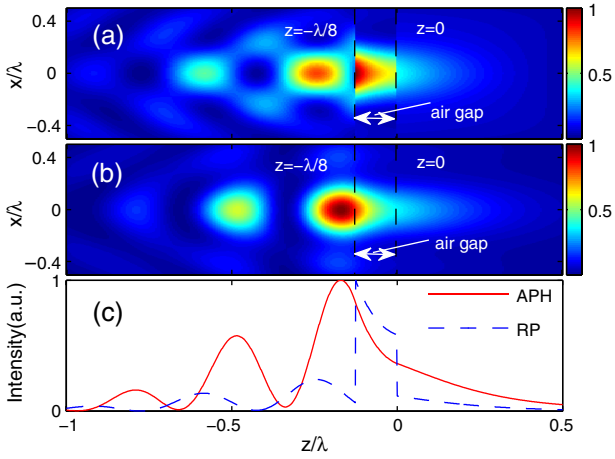

Fig. 2. (Color online) The intensity profiles in the SIL ($z < -\lambda/8$), air gap, and measured sample ($z > 0$) by the illumination of (a) RP and (b) APH. The discontinuity of intensity caused by the longitudinal field component in the RP illumination is clearly displayed by (c) the one-dimensional normalized intensity along the optical axis ($x = 0$).

In high-NA SIL-based optics, it is hard to maintain the extremely high resolution both in the SIL and measured sample simultaneously because of the inevitable air gap between the SIL and sample in the illumination of linear, circular, and radial polarization [3]. However, for the APH illumination suggested in this Letter, the subwavelength spots are both achieved in the air gap and sample in spite of the fact that the spot size (0.319λ) in the sample is slightly larger than that (0.305λ) in the air gap. For a high-NA SIL, the energy that penetrates into the sample is dominated by the evanescent wave [9]. Because of its rapid decay along the z direction, the divergence of the evanescent wave leads to the enlargement of the spot size in sample. However, the enlargement in spot size is so slight that the subwavelength spot maintains in the sample. Its advantage in reducing the focused spot size is attributed to the fact that the APH beam provides an azimuthal field component with superresolution size

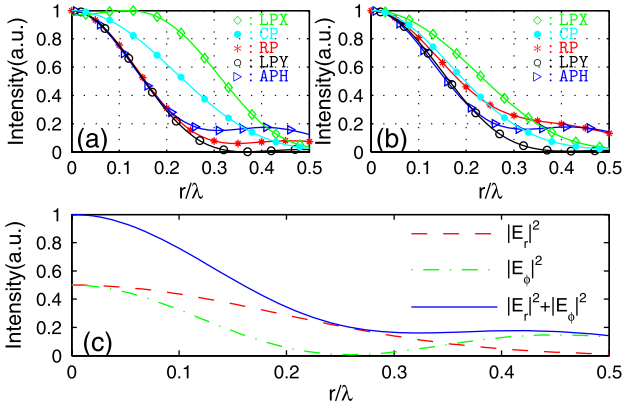

Fig. 3. (Color online) The radial intensity profiles in the transverse plane where (a) $z = -\lambda/8$ in the air gap and (b) $z = 0$ in the sample by the illumination of RP, CP, LP, and APH. LPX and LPY denote the intensity profiles along the x and y axes in the case of the LP illumination, respectively. The spot sizes are shown in Table 1. In the APH illumination, the intensity profiles of the radial, azimuthal field component and the total field where $z = 0$ in the sample are given in (c).

Table 1. Focused Spot Sizes (FWHM) Where $z = -\lambda/8$ (Plane I) in the Air Gap and $z = 0$ (Plane II) in the Sample by the Illumination of RP, CP, LP, and APH[a]

Position	LPX	CP	RP	LPY	APH
Plane I	0.639	0.477	0.311	0.307	0.305
Plane II	0.483	0.395	0.375	0.329	0.319

[a]The notations follow those in Fig. 3. The values are in units of wavelength (λ).

(0.249λ at $z = 0$ in the sample) in the focal region. After introducing the helical phase into the AP beam, one can find that the radial field component is derived in the focal region. The radial field component cannot provide a spot with superresolution size. Fortunately, the field in the focal region is not dominated by the radial field component [Fig. 3(c)]. Therefore, the total field in the focal region maintains a superresolution spot despite the fact that the spot size is still larger than that of the azimuthal field component. In addition, because the main-lobe size and intensity decrease, the side-lobe intensity in the case of APH illumination is larger than those in the case of linearly polarized (LP), circularly polarized (CP), and RP illumination [Figs. 3(a) and 3(b)]. From our above analysis, one can see that, in the case of APH illumination, the aberration induced by the near-field air gap has little influence on the resolution of the SIL system.

In the case of the APH illumination, we give the spot size (where $z = 0$) in the sample with a different refractive index in Fig. 4. One can see that the spot size has a minimum as the refractive index of the sample changes from 1.3 to 2.5. However, the spot size changes in a small range [Fig. 4(a)]. As depicted in Fig. 4, for the SILs with different NA (1.7, 1.8, and 1.9), all the spots in the sample have the superresolution size. In addition, when the well-known aperture technique is utilized [Fig. 4(b)], the spot size has little change and the difference between the maximum and minimum is smaller than 0.005λ. This means that one can choose the sample freely without suffering from the bad resolution due to the change of refractive index. However, when the aperture is used, the side-lobe intensity increases, which is the subject of our future paper. By introducing the APH illumination in the SIL-based system, we have resolved the problem that the spot size in the sample increases abruptly with the increment of the refractive index of sample in the case of RP illumination [4].

Although we suggest that the APH beam could be obtained by combining an AP and a helical phase plate, a radially polarized beam with a helical phase (RPH) has been realized experimentally by introducing a segmented half-wave plate into the laser intracavity [10]. The RPH beam can be easily converted into an APH beam by using two-cascaded $\lambda/2$ plates [1]. In fact, the APH beam, which is a new class of the Helmholtz beam, possesses a vector (polarization) and a scalar (phase) singularity simultaneously. The roles, which the vector and scalar singularity of this new class of beam have played in propagating, focusing, and interacting with materials, should be further investigated. In addition, on the basis of the given experimental devices, improving the performance of devices by introducing an incident beam with novel polarization, phase, and amplitude is still intriguing.

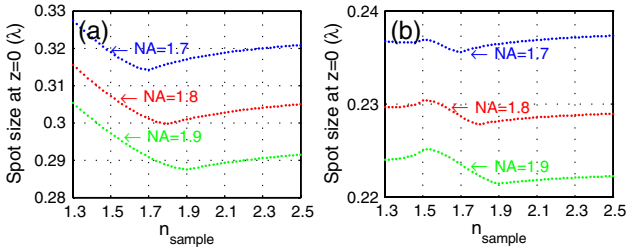

Fig. 4. (Color online) The spot size (where $z = 0$) in the sample with different refractive index when the APH illumination is adopted. The values (FWHM) (a) without and (b) with the aperture are shown. We assume that the transmission of the aperture is 0 where $0.12 < \sin\theta < 0.74$ and 1 where $\sin\theta > 0.74$ and $\sin\theta < 0.12$.

The authors thank Dr. Ren Yuxuan for his help when preparing the manuscript.

References

1. Q. W. Zhan, Adv. Opt. Photon. **1**, 1 (2009).
2. K. Huang, P. Shi, X. L. Kang, X. B. Zhang, and Y. P. Li, Opt. Lett. **35**, 965 (2010).
3. W. C. Kim, Y. J. Yoon, H. Choi, N. C. Park, and Y. P. Park, Opt. Express **16**, 13933 (2008).
4. Y. J. Yoon, W. C. Kim, N. C. Park, K. S. Park, and Y. P. Park, Opt. Lett. **34**, 1961 (2009).
5. K. S. Youngworth and T. G. Brown, Opt. Express **7**, 77 (2000).
6. X. Hao, C. F. Kuang, T. Wang, and X. Liu, Opt. Lett. **35**, 3928 (2010).
7. A. van de Nes, L. Billy, S. Pereira, and J. Braat, Opt. Express **12**, 1281 (2004).
8. B. Richards and E. Wolf, Proc. R. Soc. Lond. A **253**, 358 (1959).
9. T. D. Milster, J. S. Jo, and K. Hirota, Appl. Opt. **38**, 5046 (1999).
10. H. Kawauchi, Y. Kozawa, S. Sato, T. Sato, and S. Kawakami, Opt. Lett. **33**, 399 (2008).